International Journal of Nanomedicine

Dovepress
open access to scientific and medical research

Open Access Full Text Article

ORIGINAL RESEARCH

Silver nanoparticles embedded in zeolite membranes: release of silver ions and mechanism of antibacterial action

Amber Nagy[1]
Alistair Harrison[2]
Supriya Sabbani[3]
Robert S Munson, Jr[2]
Prabir K Dutta[3]
W James Waldman[1]

[1]Department of Pathology, The Ohio State University; [2]Center for Microbial Pathogenesis, Research Institute at Nationwide Children's Hospital, [3]Department of Chemistry, The Ohio State University, Columbus, OH, USA

Background: The focus of this study is on the antibacterial properties of silver nanoparticles embedded within a zeolite membrane (AgNP-ZM).

Methods and Results: These membranes were effective in killing *Escherichia coli* and were bacteriostatic against methicillin-resistant *Staphylococcus aureus*. *E. coli* suspended in Luria Bertani (LB) broth and isolated from physical contact with the membrane were also killed. Elemental analysis indicated slow release of Ag^+ from the AgNP-ZM into the LB broth. The *E. coli* killing efficiency of AgNP-ZM was found to decrease with repeated use, and this was correlated with decreased release of silver ions with each use of the support. Gene expression microarrays revealed upregulation of several antioxidant genes as well as genes coding for metal transport, metal reduction, and ATPase pumps in response to silver ions released from AgNP-ZM. Gene expression of iron transporters was reduced, and increased expression of ferrochelatase was observed. In addition, upregulation of multiple antibiotic resistance genes was demonstrated. The expression levels of multicopper oxidase, glutaredoxin, and thioredoxin decreased with each support use, reflecting the lower amounts of Ag^+ released from the membrane. The antibacterial mechanism of AgNP-ZM is proposed to be related to the exhaustion of antioxidant capacity.

Conclusion: These results indicate that AgNP-ZM provide a novel matrix for gradual release of Ag^+.

Keywords: silver nanoparticles, zeolite, antibacterial agent, oxidative stress

Introduction

Given that we are in an era where antibiotic resistance is a growing concern, there is a renewed interest in developing products containing silver for use as antimicrobials. For thousands of years, silver has been used for food and beverage preservation, and in medicines.[1] The use of silver as an antibacterial agent declined with the discovery of antibiotics, but the evolution of antibiotic-resistant pathogens has brought a revival in silver-based applications. Silver is now an additive in consumer products including bandages, socks, shirts, water filters, antiperspirants, combs, paints, and washing machines.[2]

The antibacterial mechanism of silver nanoparticles (AgNP) and Ag^+ has been explored extensively. Baker et al[3] found that complete bacterial cell death could be achieved at 8 μg/cm^2 AgNP and that smaller particles were more efficient antibacterials. Others have supported this finding, and found that the amount of chemisorbed Ag^+ and aggregation status of AgNP influences antibacterial efficacy.[4] The formation of reactive oxygen species has been implicated in bacterial toxicity,[5] and these are

Correspondence: Prabir K Dutta
100 West 18th Avenue, Columbus, OH 43210-1173, USA
Tel +1 614 292 4532
Fax +1 614 688 5402
Email dutta@chemistry.ohio-state.edu

submit your manuscript | www.dovepress.com
Dovepress
http://dx.doi.org/10.2147/IJN.S24019

thought to damage DNA and proteins, as well as perturb cell membrane integrity.[6]

However, there is growing concern surrounding the increasing use of AgNP and their impact of the environment. The spread of AgNP into wastewater is an environmental concern, in that researchers have found that the numbers of nitrifying bacteria found in sludge are reduced when exposed to large quantities of AgNP,[7] which has severe implications on waste water treatment.

This motivated us to develop a method to immobilize AgNP into lithographically patterned zeolite membranes, and we have already reported that such membranes are effective in killing *Escherichia coli* upon contact.[8] Other research in this area has focused on Ag^+-zeolite powders as antibacterial agents. Ag^+ ions are ion-exchanged out of the zeolite powder into media and are sufficient to cause bacterial cell death in both *E coli* and *Staphylococcus aureus*.[9,10] In the case of Ag^+-zeolite, the release of Ag^+ into solution is primarily determined by the ionic strength of the medium, because this is an ion-exchange process and is media-dependent. Recently, there has also been a report of AgNP in zeolite powders and their activity towards Gram-positive and Gram-negative bacteria.[11]

In this study, we investigated the antibacterial capacity of AgNP embedded in zeolite membranes (AgNP-ZM) and found that their bactericidal properties stem from the gradual release of Ag^+ into the media. From a materials perspective, zeolite membranes are more attractive as supports than powders, since macroscopic membranes can be grown on ceramics, metals, and polymeric and cellulose supports,[12] thus allowing for diverse applications, including use in the hospital setting. The mechanism of *E. coli* death was investigated using viability assays, gene expression arrays, and quantitative reverse transcriptase polymerase chain reaction (PCR). The biological studies suggest that exhaustion of antioxidant capacity is related to antibacterial function.

Materials and methods

Materials

Silver nitrate (99%), potassium nitrate, trypan blue, polyethylene glycol, Ludox SM-30, poly(methyl methacrylate), and hydrazine were purchased from Sigma Aldrich (St. Louis, MO). PEG-600 (Fluka, Buchs, Switzerland), Darvan (RT Vanderbilt Co Inc, Norwalk, CT), aluminum hydroxide (Alfa Aesar Ward Hill, MA, 80.5%), sodium hydroxide (Mallinckrodt Hazelwood, MO, 98.8%), 25 wt% tetramethyl ammonium hydroxide aqueous solution (Sachem, Austin, TX), AKP30 high-purity alumina powder (Sumitomo Chemical Co Ltd, Tokyo, Japan), with an average particle size of 300 nm, silastic T-2 polydimethylsiloxane (Dow Corning, Midland, MI), 200 proof ethyl alcohol (Pharmco, Brookfiled, CT), and 1-octanol (Puriss, Fluka, Buchs, Switzerland) were also purchased and used without further purification. Luria Bertani (LB) broth powder agar, brain heart-infusion broth, 100 mm sterile Petri dishes, and chloroform were obtained from Fisher Scientific (Pittsburgh, USA) and 0.4 μm pore transwell plates and six-well plates were obtained from Corning (Lowell, MA). Qiagen (Valencia, CA) supplied the Puregene DNA purification kit, the RNeasy RNA isolation kit, DNase, and QuantiTect SYBR Green reverse transcriptase PCR kit. Primers were purchased from Integrated DNA Technologies (San Diego, CA). The *E. coli* strain, XL-1 blue, which was derived from the K-12 strain, was a kind gift from Dr Joanne Trgovcich (Department of Surgery, The Ohio State University Medical Center). Bioanalyzer Lab-On-A-Chip Agilent 6000 Series II chips and E. Coli 8x15K Microarrays were purchased from Agilent (Santa Clara, CA).

Synthesis of AgNP-ZM

Macroporous alumina oxide supports were used as the substrate for zeolite membrane growth, and their preparation is described in detail in earlier studies.[13] Briefly, nanometer-sized zeolites are deposited on the alumina support and grown into a continuous membrane by hydrothermal synthesis. The zeolite membranes were then ion-exchanged with 0.005 M $AgNO_3$ solution, washed, and then reduced by hydrazine, as described earlier.[8] After washing, the AgNP-ZM were extensively ion-exchanged with 1 M NaCl to remove unreacted silver ions from the zeolite. A schematic of AgNP-ZM fabrication is provided in Supplemental Figure 1.

Chemical characterization of AgNP-ZM

Supernatants were collected from AgNP-ZM suspended in LB broth for various times and used for elemental analysis. Similar experiments were done with AgNP-ZM that were repeatedly exposed to LB broth. Silver content was measured using inductively coupled plasma optical emission spectroscopy at Galbraith Laboratories, Knoxville, TN.

Biological characterization

Cultures of XL-1 blue *E. coli* were incubated with the AgNP-ZM or zeolite membrane controls and assessed for viability using traditional colony counts. LB broth solution was prepared using a concentration of 25 g/L of LB. LB agar plates were prepared with 1.5% agar. Individual

clones were inoculated in 3 mL of LB broth and shaken at 225 rpm overnight at 37°C. Prior to exposing bacteria to the zeolite membranes, bacterial cultures were adjusted to obtain an initial optical density between 0.2 and 0.8, with viable colony counts ranging between about 1×10^5 and 1×10^8 colony-forming units (cfu)/mL. For the initial viability experiment, one zeolite membrane and one freshly prepared AgNP-ZM were tested three times. Membranes were placed into six-well tissue culture plates and 5 mL (approximately 1×10^6 cells/mL) of bacterial suspension was added to each well. Experimental plates were then incubated at 37°C and continuously shaken. For each experiment, samples were removed at 0, 30, 60, 120, and 180 minutes, where 100 µL was taken from wells containing zeolite controls or AgNP-ZM and added to a tube containing 0.9 mL of LB broth. Samples were further diluted in LB broth by 10-fold six more times. To obtain colony counts, 100 µL of samples were plated from each dilution. LB plates were incubated at 37°C overnight and cfu were counted to determine bacteria viability. Optical densities of culture supernatants were measured after exposure to two separate AgNP-ZM for 60, 120, or 180 minutes using a Shimadzu spectrophotometer at an absorbance wavelength of 600 nm.

We also tested the preliminary antibacterial activity of AgNP-ZM against a methicillin-resistant strain of *S. aureus* (MRSA, a kind gift from Dr Vijay Pancholi, Department of Pathology, The Ohio State University). Here, a clone of MRSA was grown overnight in brain-heart infusion broth. A fresh stock was inoculated into brain heart-infusion broth from the overnight culture and grown at 37°C under continuous shaking until the optical density reached 0.3. Bacterial cultures (5 mL in brain heart-infusion broth, about 5×10^7 cell/mL) were then exposed to zeolite membranes or AgNP-ZM for up to 180 minutes. Samples were taken and serially diluted as described above. Samples from each dilution (100 µL) were streaked onto brain heart-infusion agar and incubated for 24 hours at 37°C prior to counting. Zeolite membranes were reused after decontamination by steam autoclave or with 70% ethanol for 20 minutes prior to air drying.

To determine if the antibacterial action of AgNP-ZM is contact-dependent, two approaches were taken. We first exposed two AgNP-ZM and one zeolite membrane control to 5 mL of LB broth for three hours. *E. coli* (at a concentration of approximately 1×10^5 cells/mL in 5 mL of LB broth) was pelleted by centrifugation (3250 × g) for 15 minutes. The supernatants were discarded and the bacteria were resuspended in supernatants that had been exposed to the membranes. Samples were incubated at 37°C and 100 µL samples were taken at 30, 60, and 120 minutes. Colony counts were performed in the same manner as stated above, where a series of 10-fold dilutions were prepared, and 100 µL from each dilution was plated on LB agar. Plates were incubated for 24 hours at 37°C prior to counting.

To test further whether the antibacterial action of AgNP-ZM is contact-dependent, two AgNP-ZM and one zeolite membrane control were each placed in separate wells of six-well transwell plates with a membrane pore size of 0.4 µm. The membranes did not touch the bottom surface of the transwells. *E. coli* (approximately 1×10^5 cells/mL in 5 mL LB broth) was applied to the apical chamber of the transwell plates. Plates were continuously shaken and incubated at 37°C. From the apical and basal chambers, 100 µL samples were taken after 30, 60, and 120 minutes, diluted using the serial dilution scheme described above, plated, and incubated overnight at 37°C.

The efficacy of AgNP-ZM was tested by exposing the same AgNP-ZM to approximately 1×10^6 cells/mL of *E. coli* in 5 mL of LB broth a total of six times. LB broth samples (100 µL) were collected at 30, 60, and 120 minutes during each of the six experimental exposures. Colony counts were performed in the same manner stated earlier in the Materials and Methods section, where a series of 10-fold dilutions were prepared from the samples, and 100 µL from each dilution was plated on LB agar. Plates were incubated for 24 hours at 37°C prior to counting. In between each use, the AgNP-ZM were sterilized by steam autoclave, much like surgical instruments found in a hospital setting.

DNA and RNA extraction

E. coli genomic DNA was isolated using a Puregene DNA purification kit according to the manufacturer's instructions. Bacterial RNA was extracted using standard procedures from *E. coli* exposed to zeolite membranes or exposed to AgNP-ZM for 30–45 minutes (see Supplemental Methods). The quality of RNA was examined using an Agilent 2100 Bioanalyzer Lab-On-A-Chip Agilent 6000 Series II chip. RNA samples were checked for DNA contamination by running PCR using samples with primers with or without reverse transcriptase. The presence of PCR products was determined by gel electrophoresis using 1% agarose gel.

Gene expression microarrays

Four individual zeolite supports containing AgNPs and four zeolite support controls were exposed to approximately 1×10^8 cfu/mL of bacteria for 30 minutes prior to RNA

isolation, and bacterial viability was determined via colony counts (Supplemental Figure 2). RNA samples were stored at −80°C until processing. Sample labeling and hybridizations were performed by the Nationwide Children's Hospital's Biomedical Genomics Facility (http://genomics.nchresearch.org/index.html). The RNA was of high quality and all samples passed the standard quality control cutoff. Sample labeling and hybridization was performed according to the manufacturer's protocols. Samples were hybridized to the *E. coli* 8 × 15 K Microarray (AMADID 020097). Parameters regarding gene array methodology, quality control, and statistical analyses are included in the Supplemental Materials section.

Quantitative reverse transcriptase PCR

E. coli at a concentration of 1×10^8 cfu/mL were exposed to zeolite membranes alone or containing AgNPs for 45 minutes prior to RNA isolation. Quantitative reverse transcriptase PCR analyses were completed using a Quantitect SYBR Green reverse transcriptase PCR kit under the following conditions. Master mixes were prepared using 12.5 µL 2× QuantiTect SYBR Green Master Mix, 0.25 µL QuantiTect reverse transcriptase mix, and 10.25 µL RNase-free water per reaction. Forward and reverse primers were added using 0.5 µL from 25 µM stocks, and primer sequences are listed in Supplemental Table 1. Master mixes were aliquoted into 96-well plates (24 µL/well) along with 1 µL of RNA at a concentration of 1 ng/reaction. Reactions were cycled under the following conditions. Reverse transcription was performed for 30 minutes at 50°C. PCR activation was performed at 95°C for 15 minutes. Denaturation occurred at 94°C for 15 seconds, annealing occurred for 30 seconds at 58°C and extension occurred at 72°C for one minute. Cycling conditions were repeated 35 times. The ABI Prism 7500 sequence detection system was used to quantify gene expression using a gene-specific standard curve generated with bacterial DNA.

Statistical analysis

Significant differences in *E. coli* viability after incubation with AgNP-ZM and negative controls were determined by one-way analysis of variance using SigmaPlot version 11.0. For the gene expression data, bacteria were exposed to four independent zeolite membranes and four independent AgNP-ZM, and changes in expression that were two-fold or greater are considered statistically significant. In the figures, the number of AgNP-ZM used for each experiment and the statistics are included.

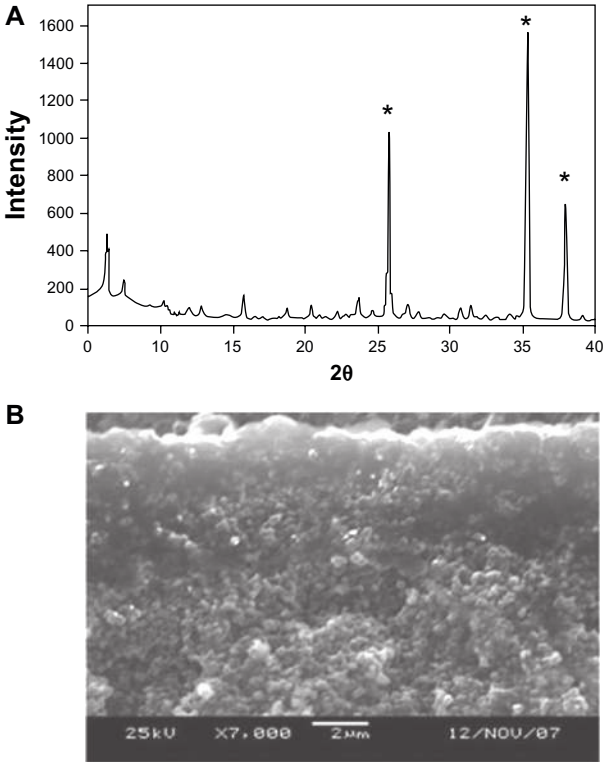

Figure 1 (**A**) Powder diffraction pattern of a zeolite membrane grown on an alumina support (the strongest peaks marked with an asterisk are due to the alumina, the rest are zeolite peaks. (**B**) Cross-section of the zeolite/alumina membrane by scanning electron microscopy.

Results

AgNP-ZM synthesis and characterization

Synthesis of AgNP-ZM starts with the synthesis of porous alumina supports, on which a seeded layer of zeolite is deposited.[13] The zeolite membrane is then grown on the seeded side via secondary hydrothermal growth. Figure 1A shows the powder x-ray pattern of a typical membrane. The three strong peaks (marked with an asterisk) arise from the alumina support. All of the other peaks are from the zeolite, the major phase being zeolite Y with minor quantities of zeolite A (strongest peak 7° 2θ). Figure 1B shows a scanning electron microscopic cross-sectional image of the membrane with the dense 2–3 µm layer of zeolite on the porous alumina (2 mm). In order to make the AgNP, the zeolite membrane is ion-exchanged with Ag^+, reduced with hydrazine to make Ag nanoclusters on the zeolite membrane, and extensively ion-exchanged with Na^+ to remove any unreacted Ag^+.[8] Figure 2A shows a scanning electron microscopic top view of the AgNP-ZM, and Figure 2B is a magnified image that clearly shows the presence of Ag clusters on the zeolite (<50 nm). Figure 2C is the elemental analysis of the surface of the membrane showing the presence of Ag, Si, and Al.

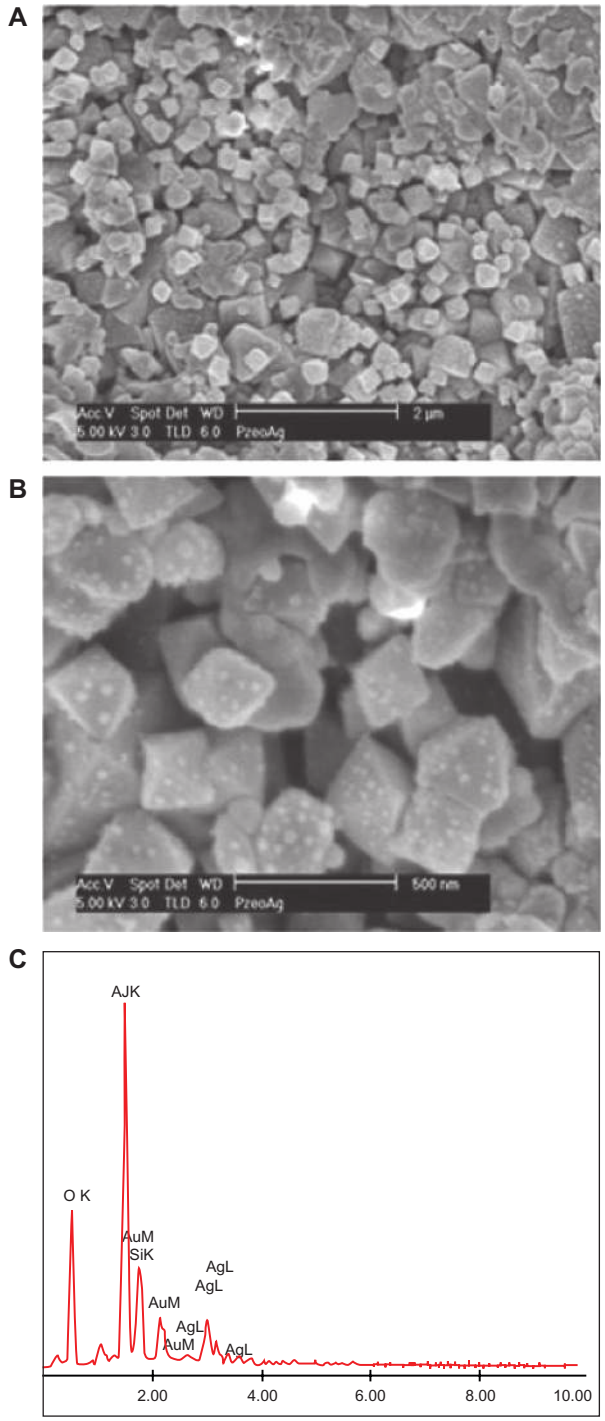

Figure 2 (**A**) Top view of the zeolite part of the silver-loaded zeolite/alumina membrane by scanning electron microscopy. (**B**) Magnified image of the top view of **A** showing discrete Ag particles on the zeolite. (**C**) Elemental analysis of the silver nanoparticles embedded in zeolite membranes, showing the presence of Ag, Si, and Al.

The AgNP-ZM were incubated in LB broth (5 mL), and the amount of Ag^+ released over time was analyzed by elemental analysis. In order to estimate an upper limit of the amount of Ag^+ that can be released from the membrane, freshly prepared (autoclaved) AgNP-ZM were exposed to LB broth for 48 hours under gentle shaking and the amount of Ag^+ was found to be approximately 20 ppm. When this same AgNP-ZM was exposed to media for 30 minutes for a second time, 5.7 ppm Ag^+ was released. After a third and fourth exposure (sample autoclaved prior to each exposure) of the same AgNP-ZM for 30-minutes and 60-minutes, contact with media released 1.9 and 1.7 ppm of Ag^+, respectively. The goal of these elemental analysis studies was to evaluate an upper limit upon single exposure for an extended time period (48 hours), and to demonstrate that the AgNP-ZM have a large reservoir of Ag (primarily due to the large internal surface area of the zeolite) so that even a second, third, and fourth exposure leads to release of Ag^+ at ppm levels.

Interaction of AgNP-ZM with *E. coli*

Antibacterial activity

E. coli was incubated alone, with a control zeolite membrane, and with a freshly prepared AgNP-ZM to determine and

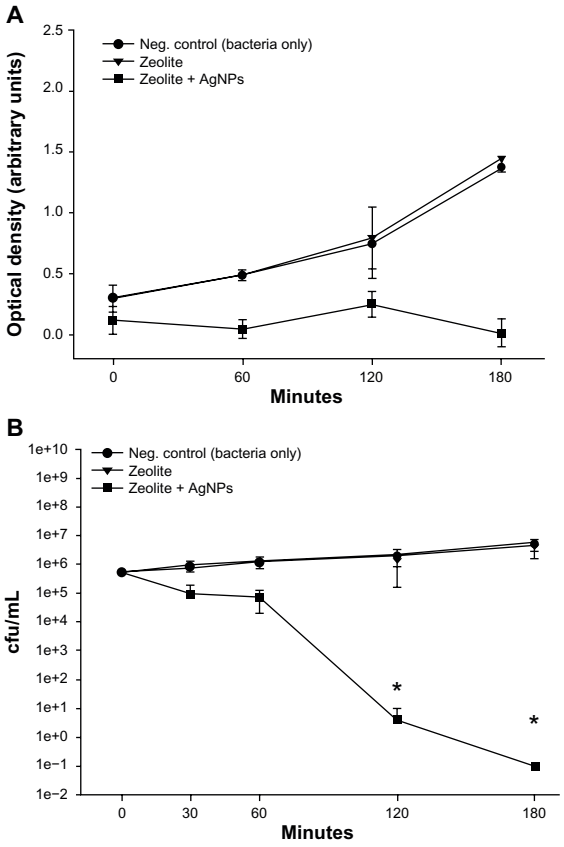

Figure 3 (**A**) Turbidity analyses of supernatant samples from unexposed *Escherichia coli* and *E. coli* exposed to zeolite controls or zeolite-supported silver nanoparticles over time. Values are expressed as the mean and standard deviation of two experiments. (**B**) Enumeration of viable *E. coli* over time upon incubation with zeolite supports containing silver nanoparticles and controls.
Notes: *Significant differences versus zeolite membrane controls, n = 3, freshly-prepared zeolite supports containing silver nanoparticles, $P < 0.05$.
Abbreviation: cfu/mL, colony forming units per milliliter.

compare the antibacterial activity of AgNP-ZM. Turbidity measurements performed on two separate occasions using freshly prepared AgNP-ZM revealed that bacterial growth was completely inhibited over a three-hour incubation period when *E. coli* was exposed to AgNP-ZM (optical density about 0.4), whereas with bacteria only and zeolite supports, proliferation increased over time, as shown in Figure 3A. Figure 3B shows the number of colonies after incubation with controls or AgNP-ZM, and a significant decrease in *E. coli* viability was observed over a three-hour period, although a decrease in bacterial viability was noted with AgNP-ZM after 30 minutes. All of the data in Figure 3B were obtained with one freshly prepared AgNP-ZM on three separate occasions.

To determine if antibacterial action was contact-dependent, a zeolite membrane control and two AgNP-ZM were incubated with 5 mL of LB broth for three hours. The membranes were then removed, and the conditioned LB broth (5 mL) was collected. Bacterial cultures which had been adjusted to about 1×10^5 cells/mL in 5 mL of LB broth were pelleted by centrifugation. The pellet was vortexed, and the conditioned broth (5 mL) was then applied to the culture. As Figure 4A shows, all *E. coli* were nonviable within 60 minutes in medium conditioned with AgNP-ZM. Medium-conditioned with zeolite membranes alone had no observable effect on bacterial viability. Figure 4B illustrates that for bacteria separated from the zeolite membranes using transwell plates containing inserts with a pore size of 0.4 µm, death was evident within 120 minutes when AgNP-ZM were used, while controls grew normally. To ensure that bacteria were unable to traverse the transwell membrane, media from the bottom chamber were sampled from all experimental treatments and plated for growth on LB agar, and no colonies were observed (data not shown).

The antibacterial activity of a single AgNP-ZM was tested a total of six times in order to evaluate the feasibility of repeated use of a membrane. The support was sterilized by steam autoclave between each use. After the AgNP-ZM had been used three or four times, the viability of *E. coli* cultures seeded at a concentration of approximately 1×10^6 cfu/mL was reduced to 0 cfu/mL within two hours (Figure 5). However, after four or more uses, complete death was apparent after three hours of incubation.

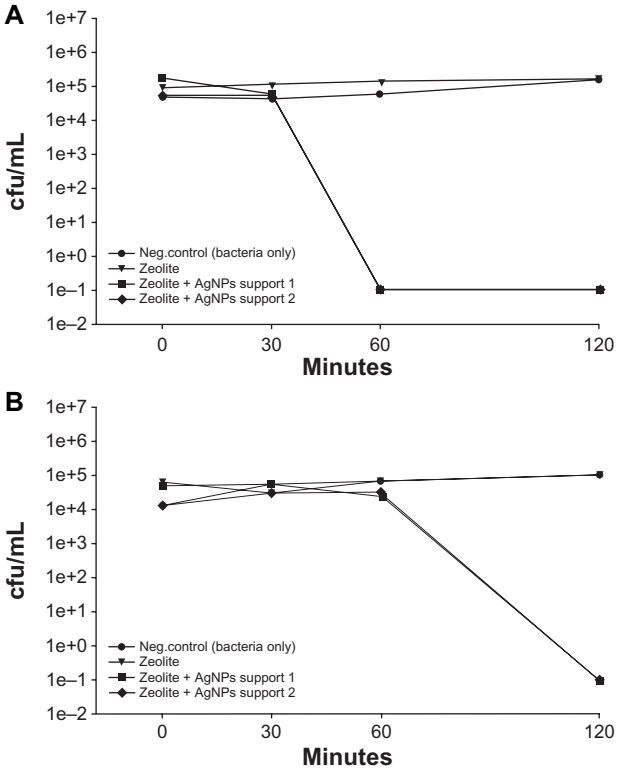

Figure 4 (**A**) Viability of *Escherichia coli* after exposure to supernatants collected from two zeolite supports containing silver nanoparticles and zeolite controls that were soaked in Luria Bertani media for three hours. (**B**) Viability of *E. coli* after exposure to two zeolite supports containing silver nanoparticles that were separated from bacteria using transwell plates. Zeolite supports containing silver nanoparticles are listed as zeolite + silver nanoparticle support 1 and support 2 in the Figure.
Abbreviation: cfu/mL, colony forming units per milliliter.

Gene expression by E. coli exposed to AgNP-ZM

Gene expression arrays revealed significant differences between *E. coli* exposed to AgNP-ZM versus zeolite membranes. A total of 145 genes were upregulated greater than two-fold, while 170 genes were downregulated (Supplemental Tables 2 and 3, respectively). Selected genes which were upregulated or downregulated by at least three-fold are included in Tables 1 and 2, respectively. Both copper transporter gene *copA* and magnesium transporter gene *mgtA* were upregulated over

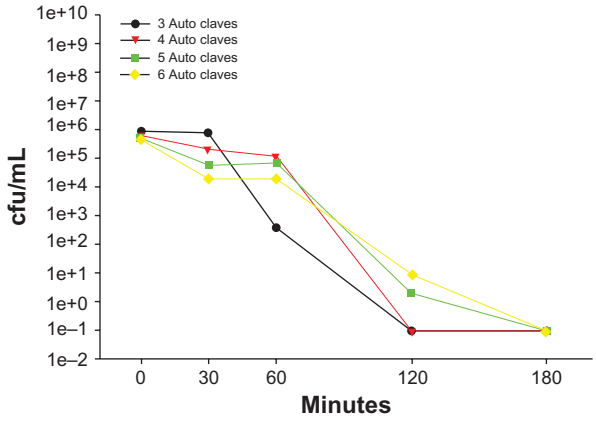

Figure 5 *Escherichia coli* at a concentration of 1×10^6 cfu/mL was incubated with the same zeolite supports containing silver nanoparticles six consecutive times, with autoclave sterilization between each use. Bacterial viability was determined using plate counts.
Abbreviation: cfu/mL, colony forming units per milliliter.

Table 1 Increases in *Escherichia coli* gene expression in response to 30-minute exposures to four independent zeolite supports containing silver nanoparticles versus *E. coli* exposed to four independent zeolite controls

Gene name	Gene product	Fold change AgNP-ZM vs zeolite	Description
cysP	Thiosulfate transporter subunit	14.9	Thiosulfate binding protein
cysW	Sulfate/thiosulfate transporter subunit	11.9	Sulfate transport system permease W protein
copA	Copper transporter	10.8	Putative ATPase
cysA	Sulfate/thiosulfate transporter subunit	10.3	ATP-binding component of sulfate permease A protein; chromate resistance
hemH	Ferrochelatase	9.5	Ferrochelatase: final enzyme of heme biosynthesis
mgtA	Magnesium transporter	9.0	Mg2+ transport ATPase, P-type 1
cysD	Sulfate adenylyltransferase, subunit 2	9.0	ATP:sulfurylase
cysU	Sulfate/thiosulfate transporter subunit	9.0	Sulfate, thiosulfate transport system permease T protein
cysJ	Sulfite reductase, alpha subunit, flavoprotein	8.7	Sulfite reductase
marA	DNA-binding transcriptional dual activator of multiple antibiotic resistance	8.1	Multiple antibiotic resistance; transcriptional activator of defense systems
zraP	Zn-binding periplasmic protein	7.9	orf, hypothetical protein
trxC	Thioredoxin 2	7.8	Putative thioredoxin-like protein
grxA	Glutaredoxin 1, redox coenzyme for ribonucleotide reductase (RNR1a)	7.6	Glutaredoxin1 redox coenzyme for glutathione-dependent ribonucleotide reductase
marR	DNA-binding transcriptional repressor of multiple antibiotic resistance	6.8	Multiple antibiotic resistance protein; repressor of mar operon
cueO	Multicopper oxidase (laccase)	6.7	orf, hypothetical protein
cysI	Sulfite reductase, beta subunit, NAD(P)-binding, heme-binding	6.1	Sulfite reductase, alpha subunit
cusF	Periplasmic copper-binding protein	5.9	orf, hypothetical protein
cysH	3′-phosphoadenosine 5′-phosphosulfate reductase	5.7	3-phosphoadenosine 5-phosphosulfate reductase
arsR	DNA-binding transcriptional repressor	5.6	Transcriptional repressor of chromosomal ars operon
arsB	Arsenite/antimonite transporter	4.2	Arsenical pump membrane protein
soxR	DNA-binding transcriptional dual regulator, Fe-S center for redox-sensing	4.2	Redox-sensing activator of soxS
arsC	Arsenate reductase	3.8	Arsenate reductase
cusB	Copper/silver efflux system, membrane fusion protein	3.1	Putative resistance protein
cusC	Copper/silver efflux system, outer membrane component	3.0	Putative resistance protein

nine-fold. The genes which encode the antioxidants thioredoxin and glutaredoxin were also upregulated greater than about 7.5-fold compared with zeolite controls. In addition, several genes encoding proteins involved with sulfur transport, ie, *cysW*, *cysA*, *cysD*, and *cysU,* were upregulated greater than nine-fold (Table 1). Genes coding for multiple antibiotic resistance (*marA* and *marR*) were increased approximately eight-fold and seven-fold, respectively (Table 1). Several genes associated with iron transport, including *fepG*, *fecR*, *fepC*, *fepA*, *fhuE*, and *fhuC*, were downregulated (Table 2), although the gene expression of *hemH* (coding for ferrochelatase) was upregulated about 10-fold (Table 1) in *E. coli* exposed to AgNP-ZM compared with zeolite membranes.

Gene expression in *E. coli* changes with AgNP-ZM use

Quantitative reverse transcriptase PCR was used to confirm gene expression microarray data. Selected genes representing those involved with metal transport, resistance, and oxidative stress were analyzed in order to identify possible mechanisms of toxicity induced by exposure to AgNP-ZM. Table 3 reports quantitative reverse transcriptase PCR data for genes encoding copper-silver efflux, glutaredoxin, multicopper oxidase, and thioredoxin, and their expression levels after each support use. With progressive use of AgNP-ZM, expression of the gene that encodes glutaredoxin decreased (fold-change of approximately 14 and 2, and virtually no change for trials 1, 2, and 3, respectively). The expression of thioredoxin was increased by approximately five-fold for *E. coli* exposed to AgNP-ZM compared with bacteria exposed to zeolite membranes alone for the first use, but for the second and third uses there was virtually no change in gene expression. Increased expression of the gene encoding multicopper oxidase remained significant with each support use, although expression decreased by approximately

Table 2 Decreases in *Escherichia coli* gene expression in response to 30-minute exposures to four independent zeolite supports containing silver nanoparticles versus *E. coli* exposed to four independent zeolite controls

Gene Name	Gene product	Fold change AgNP-ZM vs zeolite	Description
fepG	Iron-enterobactin transporter subunit	–12.6	Ferric enterobactin transport protein
fes	Enterobactin/ferric enterobactin esterase	–8.4	Enterochelin esterase
cirA	Ferric iron-catecholate outer membrane transporter	–7.1	Outer membrane receptor for iron-regulated colicin I receptor; porin; requires tonB gene product
fecR	KpLE2 phage-like element; transmembrane signal transducer for ferric citrate transport	–5.9	Regulator for fec operon, periplasmic
fepC	Iron-enterobactin transporter subunit	–5.6	ATP-binding component of ferric enterobactin transport
fes	Enterobactin/ferric enterobactin esterase	–5.6	Enterochelin esterase
fepA	Iron-enterobactin outer membrane transporter	–5.4	Outer membrane receptor for ferric enterobactin
fepD	Iron-enterobactin transporter subunit	–4.7	Ferric enterobactin
fhuE	Ferric-rhodotorulic acid outer membrane transporter	–4.0	Outer membrane receptor for ferric iron uptake
fepB	Iron-enterobactin transporter subunit	–3.7	Ferric enterobactin
sodA	Superoxide dismutase, Mn	–3.1	Superoxide dismutase, manganese
fhuC	iron-hydroxamate transporter subunit	–3.0	ATP-binding component of hydroxymate-dependent iron transport

half with latter uses (44-fold, 33-fold, and 16-fold). Gene expression of *cusC*, which encodes copper-silver efflux, fluctuated slightly with each use (approximately 2-fold, 4-fold, and 2.5-fold for trials 1, 2, and 3, respectively). These experiments were done with a single AgNP-ZM on three separate occasions.

Interaction of AgNP-ZM with other bacteria

The primary goal of this paper was to understand the interaction of AgNP-ZM with *E. coli* XL-blue, which is a laboratory strain. We also did some preliminary work using MRSA. Exposure to AgNP-ZM resulted in reduced replication, as interpreted by the lack of increase in supernatant turbidity compared with controls, although the killing efficiency of the AgNP-ZM was found to be less potent compared with *E. coli* over the same exposure period (180 minutes). These data are shown in Figure 6. The gene expression studies were performed with *E. coli*, although further experimentation is underway using other clinically relevant bacterial strains.

Discussion

The discussion primarily focuses on the properties of the AgNP-ZM and its effect on *E. coli*.

Release of Ag^+ from AgNP-ZM

In our previous study,[8] we did not address the issue of the interactions between bacteria and AgNP-ZM. Our preliminary data indicate that AgNP-ZM were bacteriostatic against MRSA, a Gram-positive clinically relevant strain of *S. aureus*. However, the bactericidal properties against this bacterium were less potent compared with Gram-negative *E. coli*. We hypothesize that cell wall differences between these two bacteria may account for the differences in bacterial

Table 3 Quantitative reverse transcriptase polymerase chain reaction analyses of select genes after three independent trials of zeolite support-containing silver nanoparticles. *Escherichia coli* at a concentration of 1×10^8 colony forming units/mL was exposed to silver nanoparticles embedded in zeolite membranes or zeolite membrane controls for 45 minutes prior to RNA isolation and analyses. Values are fold-change ± standard deviation

Gene product (*gene name*)	Gene expression fold increase		
	Zeolite supported AgNP versus zeolite control		
	Trial 1	Trial 2	Trial 3
Copper-silver efflux (*cusC*)	2.11 ± 0.02	3.93 ± 1.12	2.68 ± 0.55
Glutaredoxin (*grxA*)	14.64 ± 1.16	2.29 ± 0.26	1.22 ± 0.34
Multicopper oxidase (*cueO*)	43.90 ± 5.92	33.60 ± 0.89	16.41 ± 0.58
Thioredoxin (*trxC*)	5.30 ± 0.47	1.35 ± 0.15	0.99 ± 0.18

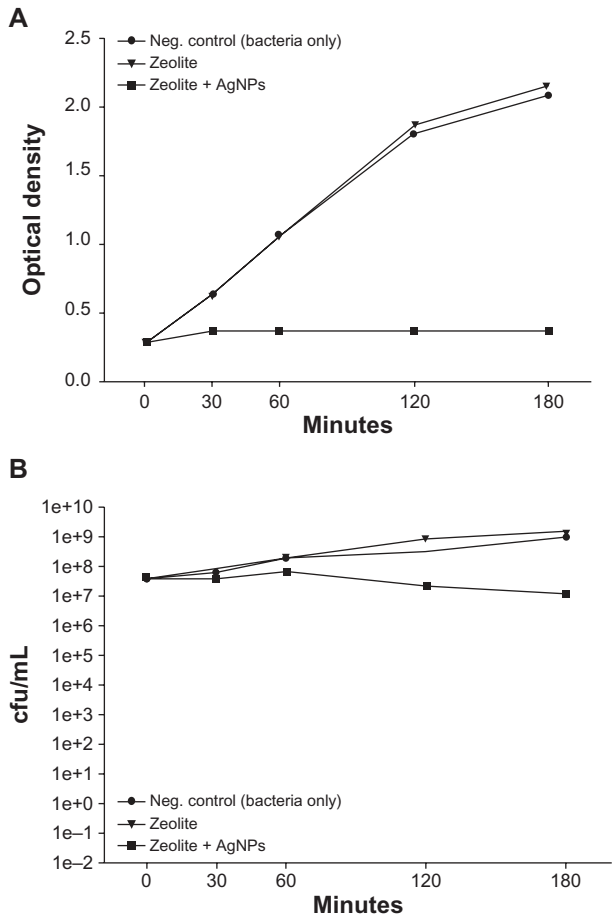

Figure 6 Growth and viability of *Staphylococcus aureus* alone, exposed to a zeolite membrane, or exposed to zeolite supports containing silver nanoparticles was evaluated over time. (**A**) Turbidity was analyzed after 30, 60, 120 or 180 minutes of exposure to a single zeolite support containing silver nanoparticles. (**B**) Bacterial viability was measured after 30, 60, 120, and 180 minutes of exposure to a single zeolite support containing silver nanoparticles.
Abbreviation: cfu/mL, colony forming units per milliliter.

viability upon exposure to AgNP-ZM, and studies are underway to investigate these findings. It is clear from the present study (Figure 4) that reduction of *E. coli* growth and viability does not require contact with the membrane. This is in contrast with the findings of Su et al,[6] who found that Ag/clay-conditioned supernatants did not have appreciable antibacterial activity. With freshly prepared AgNP-ZM, we found that the release of Ag^+ into the broth can be as high as 20 ppm after 48 hours. Since the zeolite membranes were extensively ion-exchanged with Na^+ prior to these experiments, any Ag^+ in solution would have to occur by AgNP oxidation and release. Slow release of Ag^+ from the AgNP-ZM is also supported by the observation that bacteria sequestered in the transwell plates were not killed as quickly as those incubated with supernatants conditioned for three hours (Figure 4). It is known that solutions of Ag^+ at 0.05 ppm result in complete reduction of *E. coli* viability within two hours.[14] Oxidation of AgNP over time and release of Ag^+ in less than 30 minutes has been noted.[4] With each AgNP-ZM, efficacy of the membranes decreased as well upon repeated use (Figure 5). Ag^+ released into media after the second, third, and fourth use was 5.7, 1.9, and 1.7 ppm, for 30-, 30-, and 60-minute exposures. There is clearly a decrease at the 30-minute exposure level between the second and third use, and it took twice as long (60 minutes) for the fourth use to match the release of the third use. Thus, we hypothesize that the bactericidal effects of AgNP-ZM are delayed due to reduction in the amount of Ag^+ released from AgNP-ZM with repeated use. As is evident from the scanning electron microscopy images (Figure 2B), there is a distribution of sizes of AgNP. Smaller AgNP are expected to undergo faster dissolution than larger particles, thus after each use, the Ag^+ release should decrease. In addition, autoclaving could alter the surface of the AgNP, such as the formation of insoluble hydroxides or oxides. Interestingly, it has been reported that nanosilver bandages exposed to temperatures >90°C have diminished bactericidal activity.[15] Other sterilization measures, such as ultraviolet light, are also problematic, because of the photochemistry of silver. We also used ethanol for decontamination, as reported above.

Disruption of oxidative balance

Several research groups studying AgNP have proposed that their antibacterial activity is due to the formation of reactive oxygen species. The mechanism of bacterial death was found to be a result of persistent surface free radicals found on AgNP, and that the antibacterial activity of both AgNP and Ag^+ could be reversed by n-acetylcysteine.[16] The mechanism of toxicity of AgNP in clay was proposed to be cell membrane disruption caused by the generation of reactive oxygen species, and when incubated with the antioxidant, glutathione, their viability was restored.[6] When bacterial reporter strains specifically responding to superoxide radicals were incubated with 100–300 ppm Ag^+, it was apparent that the mechanism of antibacterial activity was via reactive oxygen species, specifically superoxide, which formed after perturbation of the electron transport chain.[17] However, gene expression microarrays in the current study revealed downregulation of *sodA*, encoding a superoxide dismutase (3.1-fold decrease), which suggests that superoxide may not be the predominant reactive oxygen species driving bacterial oxidative stress. On the other hand, upregulation of expression of thioredoxin and glutaredoxin, which are crucial to maintaining oxidative balance, was noted after *E. coli* was exposed to AgNP-ZM (Table 3). Several genes associated with sulfur species trans-

port and reduction were correlated with the multiple use of the AgNP-ZM. In the presence of silver (Ag^+), bacteria may adjust sulfur pools to accommodate the synthesis of sulfur-containing antioxidants.

Genes associated with iron transport (*fep* genes) were downregulated, while *hemH*, which codes for ferrochelatase and plays an important role in heme synthesis, was upregulated. A possible response mechanism to the increased presence of Ag^+ is that the bacteria decrease the available pools of intracellular iron by increasing expression of ferrochelatase, which tightly binds Fe^{2+}, to combat and reduce oxidative stress.[18,19] The downregulation of genes with a role in iron reduction and iron release from proteins further suggests that the bacteria are attempting to control the intracellular levels of Fe^{2+},[20] thereby reducing the amount of iron available for Fenton reactions. Attempts by bacteria to regulate and restore oxidative balance are also suggested by the upregulation of *soxR*, which is involved in redox sensing and controlling expression of superoxide dismutase and other antioxidants.[21,22]

Several genes encoding for metal ion influx and intracellular metal transport and efflux were upregulated. *E. coli* exposed to AgNP-ZM upregulated *mgtA*, which encodes for proteins used for Mg^{2+} influx, and also upregulated *arsR* and *arsB,* which encode genes involved in arsenic resistance, but currently have no known role in silver toxicity. The gene *zraP*, which encodes a protein used for zinc homeostasis and *copA*, which in turn encodes for an ATPase intracellular copper transporter, were both upregulated. Others have found that *copA* is induced in the presence of silver salts,[23] but does not appear to be involved in silver resistance.[24] Thus, it is likely that the mechanisms of AgNP toxicity are similar to those for copper toxicity. Slawson et al[25] reported that Ag^+ toxicity was reduced when Cu^{2+} is also present, indicating that silver may compete with copper for entry into the cell. There appears to be some promiscuity of bacterial metal transport proteins, the functions of which have not been fully elucidated.

Developing resistance to silver

The genes known to encode silver resistance in *E. coli* are *ybdE, ylcD*, *ylcC*, *ylcB*, *ylcA*, and *ybcZ*.[26] Most silver-resistant bacterial strains have developed tolerance by utilizing Ag^+ ATPase efflux pumps and antiporters rather than chemical detoxification mechanisms.[27] However, in the current study, only *cusC (ylcB)* and *cusF (ylcC)*, the genes encoding for copper-silver efflux outer membrane protein and periplasmic copper and silver binding proteins, respectively, were upregulated when the bacteria were exposed to AgNP-ZM as compared with zeolite membrane controls. Further, we were able to confirm the upregulation of copper-silver efflux outer membrane protein (*cusC*) gene transcripts using quantitative reverse transcriptase PCR, although expression levels fluctuated with AgNP-ZM use, which may be a result of variations in Ag^+ release. The increase in gene transcription of multiple antibiotic resistant genes *marA* and *marR* is remarkable. The increased expression of *mar* genes is associated with antibiotic resistance (including tetracycline and ampicillin resistance).[28] This work indicates that multiple antibiotic resistance genes may also play a role in the evolution of silver resistance in *E. coli*, and warrant further investigation.

Conclusion

The concept of using intrazeolitic space for storage of specific molecules and their slow release has found many applications. For example, controlled release of the preservative, cresol, from zeolite was successfully demonstrated by Erikkson[29] where *E. coli* and *S. aureus* viability was reduced. Another study demonstrated the feasibility of zeolites as a vehicle for drug delivery by releasing ketoprofen under different physiological conditions.[30] We have shown that surface-modified zeolites can release paraquat under controlled conditions.[31] However, this study is the first to demonstrate that zeolite membranes can serve as supports, and we demonstrate this functionality using AgNP for antibacterial use. The impact of using membranes is that such membranes can be grown on various supports, including plastics, cellulose, and metals.[12] Possible uses of this technology could include antibacterial coatings for a wide variety of applications. Further, these membranes have the propensity to be tailored for controlled release, thus dictating the amount of cargo released into the environment. Gene expression studies suggest that the mechanism for the antibacterial activity of AgNP-ZM is centered around the depletion of cellular antioxidant capacity by gradual release of Ag^+ from zeolite membranes.

Acknowledgments

Support for this research was obtained through grants from the National Institute for Occupational Safety and Health and US Department of Agriculture/National Institute of Food and Agriculture. We are grateful to Drs Vijay Pancholi and Joanne Trgovcich for donating the bacterial cultures used in this study. We thank David Newsom and Dr Peter White at the Nationwide Children's Hospital's Biomedical Genomics Core for their assistance with the gene expression microarray assays and analyses.

Disclosure

The authors report no conflicts of interest in this work.

References

1. Alexander JW. History of the medical use of silver. *Surg Infect*. 2009; 10(3):289–292.
2. Chen X, Schluesener HJ. Nanosilver: A nanoproduct in medical application. *Toxicol Lett*. 2008;176(1):1–12.
3. Baker C, Pradhan A, Pakstis L, Pochan DJ, Shah SI. Synthesis and antibacterial properties of silver nanoparticles. *J Nanosci Nanotechnol*. 2005;5(2):244–249.
4. Lok CN, Ho CM, Chen R, et al. Silver nanoparticles: Partial oxidation and antibacterial activities. *J Biol Inorg Chem*. 2007;12(4):527–534.
5. Choi O, Hu Z. Size dependent and reactive oxygen species related nanosilver toxicity to nitrifying bacteria. *Environ Sci Technol*. 2008;42(12):4583–4588.
6. Su HL, Chou CC, Hung DJ, et al. The disruption of bacterial membrane integrity through ROS generation induced by nanohybrids of silver and clay. *Biomaterials*. 2009;30(30):5979–5987.
7. Liang Z, Das A, Hu Z. Bacterial response to a shock load of nanosilver in an activated sludge treatment system. *Water Res*. 2010;44(18): 5432–5438.
8. Sabbani S, Gallego-Perez D, Nagy A, Waldman WJ, Hansford D, Dutta PK. Synthesis of silver-zeolite films on micropatterned porous alumina and its application as an antimicrobial substrate. *Micropor Mesopor Mat*. 2010;135(1–3):131–136.
9. Fernández A, Soriano E, Hernández-Muñoz P, Gavara R. Migration of antimicrobial silver from composites of polylactide with silver zeolites. *J Food Sci*. 2010;75(3):E186–E193.
10. Kwakye-Awuah B, Williams C, Kenward MA, Radecka I. Antimicrobial action and efficiency of silver-loaded zeolite X. *J Appl Microbiol*. 2008;104(5):1516–1524.
11. Shameli K, Ahmad MB, Zargar M, Yunus WM, Ibrahim NA. Fabrication of silver nanoparticles doped in the zeolite framework and antibacterial activity. *Int J Nanomedicine*. 2011;(6):331–341.
12. Tavolaro A, Drioli E. Zeolite membranes. *Adv Mater*. 1999;11: 975–996.
13. White JC, Dutta PK, Shqau K, Verweij H. Synthesis of ultrathin zeolite Y membranes and their application for separation of carbon dioxide and nitrogen gases. *Langmuir*. 2010;(26):10287–10293.
14. Jung WK, Koo HC, Kim KW, Shin S, Kim SH, Park YH. Antibacterial activity and mechanism of action of the silver ion in Staphylococcus aureus and Escherichia coli. *Appl Environ Microbiol*. 2008;74(7): 2171–2178.
15. Landry BK, Nadworny PL, Omotoso OE, Maham Y, Burrell JC, Burrell RE. The kinetics of thermal instability in nanocrystalline silver and the effect of heat treatment on the antibacterial activity of nanocrystalline silver dressings. *Biomaterials*. 2009;30(36):6929–6939.
16. Kim JS, Kuk E, Yu KN, et al. Antimicrobial effects of silver nanoparticles. *Nanomed Nanotech Biol Med*. 2007;3(1):95–101.
17. Park HJ, Kim JY, Kim J, et al. Silver-ion-mediated reactive oxygen species generation affecting bactericidal activity. *Water Res*. 2009;43(4): 1027–1032.
18. Crichton RR, Wilmet S, Legssyer R, Ward RJ. Molecular and cellular mechanisms of iron homeostasis and toxicity in mammalian cells. *J Inorg Biochem*. 2002;91(1):9–18.
19. Hunter GA, Sampson MP, Ferreira GC. Metal ion substrate inhibition of ferrochelatase. *J Biol Chem*. 2008;283(35):23685–23691.
20. Andrews SC. Iron storage in bacteria. *Adv Microb Physiol*. 1998;40: 281–351.
21. Ha U, Jin S. Expression of the soxR gene of Pseudomonas aeruginosa is inducible during infection of burn wounds in mice and is required to cause efficient bacteremia. *Infect Immun*. 1999;67(10):5324–5331.
22. Gort AS, Imlay JA. Balance between endogenous superoxide stress and antioxidant defenses. *J Bacteriol*. 1998;180(6):1402–1410.
23. Rensing C, Fan B, Sharma R, Mitra B, Rosen BP. CopA: An Escherichia coli Cu(I)-translocating P-type ATPase. *Proc Natl Acad Sci U S A*. 2000;97(2):652–656.
24. Franke S, Grass G, Nies DH. The product of the ybdE gene of the Escherichia coli chromosome is involved in detoxification of silver ions. *Microbiology*. 2001;147(4):965–972.
25. Slawson RM, Lee H, Trevors JT. Bacterial interactions with silver. *BioMetals*. 1990;3(3):151–154.
26. Silver S, Phung le T, Silver G. Silver as biocides in burn and wound dressings and bacterial resistance to silver compounds. *J Ind Microbiol Bio technol*. 2006;33(7):627–634.
27. Silver S. Bacterial silver resistance: Molecular biology and uses and misuses of silver compounds. *FEMS Microbiol Rev*. 2003;27(2–3): 341–353.
28. Okusu H, Ma D, Nikaido H. AcrAB efflux pump plays a major role in the antibiotic resistance phenotype of Escherichia coli multiple-antibiotic-resistance (Mar) mutants. *J Bacteriol*. 1996;178(1):306–308.
29. Eriksson H. Controlled release of preservatives using dealuminated zeolite Y. *J Biochem Biophys Methods*. 2008;70(6):1139–1144.
30. Rimoli MG, Rabaioli MR, Melisi D, et al. Synthetic zeolites as a new tool for drug delivery. *J Biomed Mater Res A*. 2008;87(1):156–164.
31. Zhang H, Kim Y, Dutta PK. Controlled release of paraquat from surface-modified zeolite Y. *Micropor Mesopor Mat*. 2006;88(1–3):312–318.

Supplemental Methods

RNA isolation

Bacteria were collected from each well and pelleted at 4°C in 15 mL centrifuge tubes at 3250 × g for 15 minutes. Supernatants were discarded and the pellets were homogenized in 5 mL Trizol for five minutes. Each tube was shaken vigorously for 30 seconds after the addition of 1 mL of chloroform. The tubes were incubated at room temperature for three minutes prior to centrifugation at 4°C and 3250 × g for 15 minutes. The organic layer was then removed and placed into clean RNase free microfuge tubes. Equal amounts of 100% ethanol were added to each tube and mixed by pipetting. RNA purification was then performed using RNeasy mini kits as per the manufacturer's instructions, during which DNase was added to remove contaminating DNA. At the final elution step, RNA was resuspended in 20 µL of RNase-free H_2O and stored at −80°C until further use in gene expression arrays and quantitative reverse transcription polymerase chain reaction experiments. The concentration of the samples provided was determined using the NanoDrop® ND-1000 ultraviolet-visible spectrophotometer.

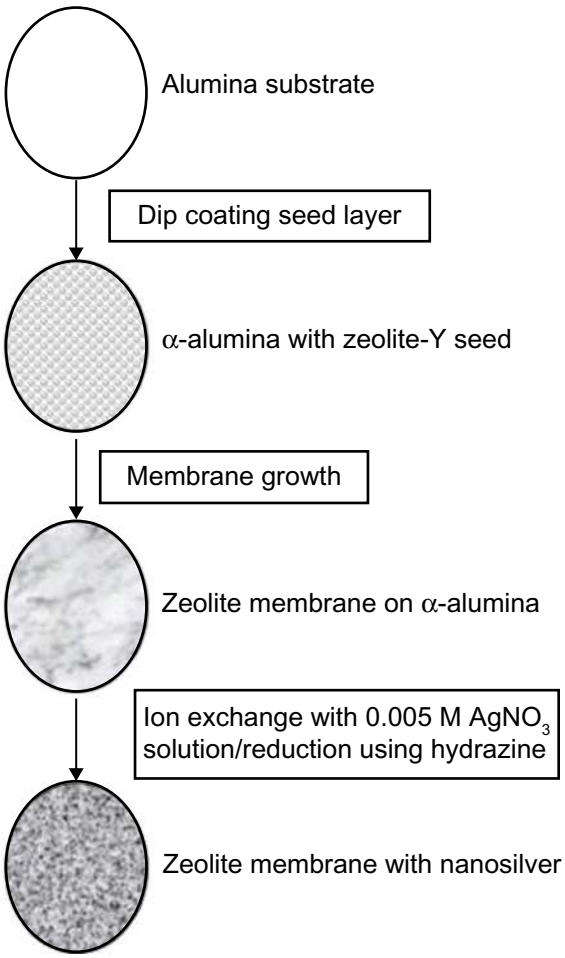

Figure S1 Schematic of fabrication of zeolite support containing silver nanoparticles. Alumina supports were used as the substrate for zeolite membrane synthesis. Zeolite was grown into a continuous membrane by hydrothermal synthesis. Zeolite membranes were then ion-exchanged with 0.005 M $AgNO_3$ solution, washed, and then reduced by hydrazine.

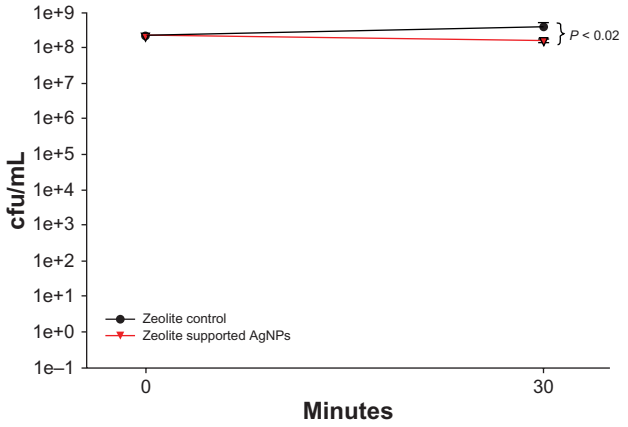

Figure S2 Viability of *Escherichia coli* after exposure to zeolite support containing silver nanoparticles for 30 minutes. The viability of *E. coli* was determined after exposure to zeolite support containing silver nanoparticles for 30 minutes. RNA was harvested from these experiments and used for the gene expression microarray analyses. Viability was significantly reduced after incubation with zeolite support containing silver nanoparticles for 30 minutes, compared with zeolite controls. Statistical significance was determined using the Student's *t*-test (n = 4 for zeolite controls and zeolite support containing silver nanoparticles, $P < 0.02$).

Gene arrays

Microarray slides were hybridized overnight, washed, and then scanned with an Agilent G2505C microarray scanner. This high-resolution scanner features an industry-leading extended dynamic range of 10^6 (20-bits) for high sensitivity scanning without saturation, low-level detection resulting from optimized precision optics, broad dynamic range, and minimal spectral cross talk that enables detection of weak features. The information about each probe on the array was extracted from the image data using Agilent Feature Extraction 10.9. This data was stored in Feature Extraction ".txt" files. The raw intensity values from these files were imported into the mathematical software package "R", which is used for all data input, diagnostic plots, normalization, and quality checking steps of the analysis process using scripts developed inhouse specifically for this analysis. These scripts call on several Bioconductor packages (http://www.bioconductor.org/). Bioconductor is an open source and open development software project that provides tools for the analysis and comprehension of genomic data.[1] Significance analyses of microarrays (SAM) is a powerful tool for analyzing microarray gene expression data useful for identifying differentially expressed genes between two conditions.[2] SAM was used to calculate a test

Table S1 *E. coli* primer sequences for quantitative real-time PCR (QRT-PCR)

Gene product (*gene name*)	Sequence	T_m(C)	Product size
Multi copper oxidase (*cueO*) F	TTCCGTATCTTGTCAGAAAATGGCA	58.7	195 bp
Multi copper oxidase (*cueO*) R	TACCGTAAACCCTAACATCATCCCC	58.2	
Thioredoxin (*trxC*) F	ACACTCGACAAATTGCTGAAGGATG	58.3	164 bp
Thioredoxin (*trxC*) R	AATTCACGTTCAGCTTCGGTATTCAC	58.7	
Glutaredoxin (*grxA*) F	TTGCCCTTACTGTGTGCGTGC	58.4	151 bp
Glutaredoxin (*grxA*) R	CGGCACGGTTTCTACGGGTT	58.5	
Copper/silver efflux (*cusC*) F	TTATGAACAGAAAATCCAGAACGCCT	58.3	228 bp
Copper/silver efflux (*cusC*) R	TAATTCAGATCAAGTAAAGTTTGTCGGGT	58	

Abbreviations: F = Forward sequence; R = Reverse sequence; bp = base pairs.

statistic for relative difference in gene expression based on permutation analysis of expression data and calculated a false discovery rate using the q-value method presented by Storey and Tibshirani.[3] In outline, SAM identified statistically significant genes by carrying out gene-specific *t*-tests and computed a statistic for each gene. This test statistic measured the strength of the relationship between gene expression and a five-response variable. This analysis used no-parametric statistics, given that the data may not follow a normal distribution. The response variable described and grouped the data based on experimental conditions. In this method, repeated permutations of the data were used to determine if the expression of any gene is significantly related to the response. The use of permutation-based analysis accounted for correlations in genes and avoided parametric assumptions about the distribution of individual genes. For this experiment, SAM analysis was implemented in R using the Bioconductor Siggenes package. Also, Relative Log Expression values were computed for each probe set by comparing the expression value in each array against the median expression value for that probe set across all arrays. Gene expression arrays were analyzed using a 10% false discovery rate to generate the list of significantly differentially expressed genes. The q-values (false discovery rate) for each gene are provided in the results table, and the lower the value the more significant the result.

Table S2 Increases in *E. coli* gene expression in response to 30-minute exposures to four independent zeolite supports containing AgNPs versus *E. coli* exposed to four independent zeolite controls

Gene product	Fold change AgNP-ZM vs zeolite	Description
Thiosulfate transporter subunit	14.9	Thiosulfate binding protein
Predicted protein	14.6	Multiple antibiotic resistance protein
Predicted transcriptional regulator	13	orf, hypothetical protein
Sulfate/thiosulfate transporter subunit	11.9	Sulfate transport system permease W protein
Copper transporter	10.8	Putative ATPase
Sulfate/thiosulfate transporter subunit	10.3	ATP-binding component of sulfate permease A protein; chromate resistance
Ferrochelatase	9.5	Ferrochelatase: final enzyme of heme biosynthesis
Magnesium transporter	9	Mg2+ transport ATPase, P-type 1
Sulfate adenylyltransferase, subunit 2	9	ATP:sulfurylase
Sulfate/thiosulfate transporter subunit	9	Sulfate, thiosulfate transport system permease T protein
Predicted DNA-binding transcriptional regulator	8.8	orf, hypothetical protein
Sulfite reductase, alpha subunit, flavoprotein	8.7	Sulfite reductase
DNA-binding transcriptional dual activator of multiple antibiotic resistance	8.1	Multiple antibiotic resistance; transcriptional activator of defense systems
Predicted inner membrane protein	8.1	Putative transport system permease protein
Conserved protein	8	orf, hypothetical protein
Predicted protein	7.9	orf, hypothetical protein
Zn-binding periplasmic protein	7.9	orf, hypothetical protein
Pseudo	7.8	Attaching and effacing protein, pathogenesis factor
Thioredoxin 2	7.8	Putative thioredoxin-like protein

(*Continued*)

Table S2 (*Continued*)

Gene product	Fold change AgNP-ZM vs zeolite	Description
Glutaredoxin 1, redox coenzyme for ribonucleotide reductase (RNR1a)	7.6	Glutaredoxin1 redox coenzyme for glutathione-dependent ribonucleotide reductase
Sulfate transporter subunit	7.6	Periplasmic sulfate-binding protein
Predicted oxidoreductase with NAD(P)-binding Rossmann-fold domain	7.2	Putative oxidoreductase
Predicted cyanide hydratase	7.1	orf, hypothetical protein
5,10-methylenetetrahydrofolate reductase	7.1	5,10-methylenetetrahydrofolate reductase
DNA-binding transcriptional repressor of multiple antibiotic resistance	6.8	Multiple antibiotic resistance protein; repressor of mar operon
Multicopper oxidase (laccase)	6.7	orf, hypothetical protein
Sulfite reductase, beta subunit, NAD(P)-binding, heme-binding	6.1	Sulfite reductase, alpha subunit
Predicted quinol oxidase subunit	6	orf, hypothetical protein
Predicted protein	5.9	orf, hypothetical protein
Periplasmic copper-binding protein	5.9	orf, hypothetical protein
Alkyl hydroperoxide reductase, F52a subunit, FAD/NAD(P)-binding	5.8	Alkyl hydroperoxide reductase, F52a subunit; detoxification of hydroperoxides
Predicted DNA-binding transcriptional regulator	5.8	orf, hypothetical protein
DNA-binding transcriptional activator, homocysteine-binding	5.7	Regulator for metE and metH
3′-phosphoadenosine 5′-phosphosulfate reductase	5.7	3-phosphoadenosine 5-phosphosulfate reductase
DNA-binding transcriptional repressor	5.6	Transcriptional repressor of chromosomal ars operon
IS1 transposase InsAB'	5.6	IS1 protein InsB
Conserved protein	5.4	orf, hypothetical protein
Conserved protein	5	orf, hypothetical protein
Predicted membrane protein	4.9	orf, hypothetical protein
Sulfate adenylyltransferase, subunit 1	4.9	ATP-sulfurylase
Predicted protein	4.4	orf, hypothetical protein
Alcohol dehydrogenase class III/glutathione-dependent formaldehyde dehydrogenase	4.4	Alcohol dehydrogenase class III; formaldehyde dehydrogenase
N-ethylmaleimide reductase, FMN-linked	4.3	N-ethylmaleimide reductase
Conserved protein	4.3	orf, hypothetical protein
RNA polymerase, sigma 32 (sigma H) factor	4.3	RNA polymerase, sigma
Nitrate reductase 1, beta (Fe-S) subunit	4.2	Nitrate reductase 1, beta subunit
Arsenite/antimonite transporter	4.2	Arsenical pump membrane protein
DNA-binding transcriptional dual regulator, Fe-S center for redox-sensing	4.2	Redox-sensing activator of soxS
Respiratory NADH dehydrogenase 2/cupric reductase	3.9	Respiratory NADH dehydrogenase
Predicted inner membrane protein, part of terminus	3.9	Putative transport protein
Envelope stress induced periplasmic protein	3.8	Periplasmic protein related to spheroblast formation
Fused fructose-specific PTS enzymes: IIA component/HPr component	3.8	PTS system, fructose-specific IIA/fpr component
Arsenate reductase	3.8	Arsenate reductase
Fructose-1-phosphate kinase	3.6	Fructose-1-phosphate kinase
DNA-binding transcriptional repressor	3.6	orf, hypothetical protein
Predicted transporter	3.6	Part of a kinase
Nitrate reductase 1, alpha subunit	3.6	Nitrate reductase 1, alpha subunit
Predicted esterase	3.5	Putative esterase
Molybdenum-cofactor-assembly chaperone subunit of nitrate reductase 1	3.5	Nitrate reductase 1, delta subunit, assembly function
3-oxoacyl-[acyl-carrier-protein] synthase II	3.4	3-oxoacyl-
DL-methionine transporter subunit	3.3	ATP-binding component of a transporter
Predicted (D)-galactarate transporter	3.3	Putative transport protein
Fused chorismate mutase T/prephenate dehydrogenase	3.3	Chorismate mutase-T and prephenate dehydrogenase
Nitrate reductase 1, gamma (cytochrome b(NR)) subunit	3.2	Nitrate reductase 1, cytochrome b
Fumarate hydratase (fumarase C), aerobic Class II	3.2	Fumarase C= fumarate hydratase Class II; isozyme
Copper/silver efflux system, membrane fusion protein	3.1	Putative resistance protein

(*Continued*)

Table S2 (*Continued*)

Gene product	Fold change AgNP-ZM vs zeolite	Description
Membrane protein of efflux system	3.1	orf, hypothetical protein
Copper/silver efflux system, outer membrane component	3	Putative resistance protein
Regulator protein that represses frmRAB operon	3	Putative alpha helix chain
Homoserine O-transsuccinylase	3	Homoserine transsuccinylase
Predicted pirin-related protein	3	orf, hypothetical protein
Fused nitric oxide dioxygenase/dihydropteridine reductase 2	3	Dihydropteridine reductase, ferrisiderophore reductase activity
Nitrite reductase, large subunit, NAD(P)H-binding	2.9	Nitrite reductase
Predicted inner membrane protein	2.9	Putative transport protein
Adenosine 5'-phosphosulfate kinase	2.8	Adenosine 5-phosphosulfate kinase
Maltose regulon periplasmic protein	2.8	Periplasmic protein of mal regulon
Conserved protein	2.8	orf, hypothetical protein
Carbon-phosphorus lyase complex subunit	2.8	Phosphonate metabolism
Maltose transporter subunit	2.7	Periplasmic maltose-binding protein; substrate recognition for transport and chemotaxis
Fructuronate transporter	2.7	Gluconate transport system permease 3
Predicted regulator of cell morphogenesis and cell wall metabolism	2.6	orf, hypothetical protein
DNA-binding transcriptional dual regulator, glycolate-binding	2.6	Transcriptional activator for glc operon
Predicted endopeptidase	2.6	Heat shock protein, integral membrane protein
Conserved protein	2.6	orf, hypothetical protein
Formate dehydrogenase-N, Fe-S (beta) subunit, nitrate-inducible	2.6	Formate dehydrogenase-N, nitrate-inducible, iron-sulfur beta subunit
Predicted glucarate dehydratase	2.6	Putative glucarate dehydratase
Calcium/sodium:proton antiporter	2.5	Sodium-calcium/proton antiporter
Formate dehydrogenase-N, alpha subunit, nitrate-inducible	2.5	Formate dehydrogenase-N, nitrate-inducible, alpha subunit
Gluconate transporter, high-affinity GNT I system	2.5	High-affinity transport of gluconate/gluconate permease
Predicted peptidoglycan peptidase	2.5	orf, hypothetical protein
Formate dehydrogenase-N, cytochrome B556 (gamma) subunit, nitrate-inducible	2.4	Formate dehydrogenase-N, nitrate-inducible, cytochrome B556
e14 prophage; predicted DNA-binding transcriptional regulator	2.4	orf, hypothetical protein
Nitrite reductase, NAD(P)H-binding, small subunit	2.4	Nitrite reductase
Predicted zinc-dependent peptidase	2.4	orf, hypothetical protein
Conserved protein required for cell growth	2.4	orf, hypothetical protein
Cystathionine gamma-synthase, PLP-dependent	2.4	Cystathionine gamma-synthase
Conserved protein	2.4	orf, hypothetical protein
L-serine deaminase I	2.4	L-serine deaminase
Predicted reductase	2.4	Putative reductase
Alpha-dehydro-beta-deoxy-D-glucarate aldolase	2.4	orf, hypothetical protein
D-serine ammonia-lyase	2.4	D-serine dehydratase
Serine endoprotease (protease Do), membrane-associated	2.3	Periplasmic serine protease Do; heat shock protein HtrA
NADH-azoreductase, FMN-dependent	2.3	Acyl carrier protein phosphodiesterase
Isopentenyl diphosphate isomerase	2.3	Putative enzyme
Nitrite reductase, NAD(P)H-binding, small subunit	2.3	Nitrite reductase
Porphobilinogen synthase	2.3	5-aminolevulinate dehydratase = porphobilinogen synthase
Fused predicted pyruvate-flavodoxin oxidoreductase	2.3	Putative oxidoreductase, Fe-S subunit
Nitrite reductase, NAD(P)H-binding, small subunit	2.3	Nitrite reductase
Sorbitol-6-phosphate dehydrogenase	2.3	Glucitol
e14 prophage; predicted DNA-binding transcriptional regulator	2.3	orf, hypothetical protein
Inhibitor of replication at Ter, DNA-binding protein	2.2	DNA-binding protein; inhibition of replication at Ter sites
Glycerol-3-phosphate O-acyltransferase	2.2	Glycerol-3-phosphate acyltransferase
Predicted DNA-binding transcriptional regulator	2.2	orf, hypothetical protein
(D)-glucarate dehydratase I	2.2	Putative glucarate dehydratase
Sodium:serine/threonine symporter	2.2	Putative transport protein
Conserved protein	2.2	orf, hypothetical protein

(*Continued*)

Table S2 (*Continued*)

Gene product	Fold change AgNP-ZM vs zeolite	Description
D-xylose transporter	2.2	Xylose-proton symport
Sodium-proton antiporter	2.2	Na+/H antiporter, pH dependent
Endonuclease IV with intrinsic 3'-5' exonuclease activity	2.2	Endonuclease IV
Pseudo	2.2	Putative transport system permease protein
Conserved protein	2.2	orf, hypothetical protein
KpLE2 phage-like element; IS2 insertion element transposase InsAB'	2.2	IS2 hypothetical protein
4-alpha-glucanotransferase (amylomaltase)	2.1	4-alpha-glucanotransferase
Predicted transporter subunit: periplasmic-binding component of ABC superfamily	2.1	Putative transport periplasmic protein
Predicted DNA-binding transcriptional regulator	2.1	Putative transcriptional regulator LYSR-type
Conserved protein	2.1	orf, hypothetical protein
Catalase/hydroperoxidase HPI(I)	2.1	Catalase; hydroperoxidase HPI
Crotonobetaine reductase subunit II, FAD-binding	2.1	Probable carnitine operon oxidoreductase
CP4-6 prophage; predicted ferric transporter subunit	2.1	Putative ATP-binding component of a transport system
Exonuclease III	2.1	Exonuclease III
Dihydroxyacid dehydratase	2.1	Dihydroxyacid dehydratase
Sn-glycerol-3-phosphate dehydrogenase, aerobic, FAD/NAD(P)-binding	2.1	Sn-glycerol-3-phosphate dehydrogenase
Fused DNA-binding response regulator in two-component regulatory system with Zra	2.1	Response regulator of hydrogenase 3 activity
Nitrite reductase, NAD(P)H-binding, small subunit	2.1	Nitrite reductase
3-deoxy-D-arabino-heptulosonate-7-phosphate synthase, tyrosine-repressible	2.1	3-deoxy-D-arabinoheptulosonate-7-phosphate synthase
Conserved inner membrane protein	2.1	orf, hypothetical protein
DNA-binding protein, hemimethylated	2	orf, hypothetical protein
Conserved protein	2	Putative receptor
Conserved inner membrane protein	2	orf, hypothetical protein
Dihydroxyacetone kinase, C-terminal domain	2	Putative dihydroxyacetone kinase
Predicted transporter subunit: ATP-binding component of ABC superfamily	2	Putative ATP-binding component of a transport system

Table S3 Decreases in *Escherichia coli* gene expression in response to 30-minute exposures to four independent zeolite supports containing silver nanoparticles versus *E. coli* exposed to four independent zeolite controls

Gene name	Gene product	Fold change AgNP-ZM vs zeolite	Description
fliQ	Flagellar biosynthesis protein	–2	Flagellar biosynthesis
mdtQ	Pseudo	–2	orf, hypothetical protein
yhdE	Conserved protein	–2	orf, hypothetical protein
yciT	Predicted DNA-binding transcriptional regulator	–2	Putative DEOR-type transcriptional regulator
yjcC	Predicted signal transduction protein (EAL domain containing protein)	–2	orf, hypothetical protein
yehE	Predicted protein	–2	orf, hypothetical protein
sdiA	DNA-binding transcriptional activator	–2	Transcriptional regulator of ftsQAZ gene cluster
yeeA	Conserved inner membrane protein	–2	orf, hypothetical protein
yncH	Predicted protein	–2	orf, hypothetical protein
ndk	Multifunctional nucleoside diphosphate kinase	–2	Nucleoside diphosphate kinase
yebW	Predicted protein	–2	orf, hypothetical protein
ycjW	Predicted DNA-binding transcriptional regulator	–2	Putative LACI-type transcriptional regulator

(*Continued*)

Table S3 (*Continued*)

Gene name	Gene product	Fold change AgNP-ZM vs zeolite	Description
ycgN	Conserved protein	−2.1	orf, hypothetical protein
alsA	Fused D-allose transporter subunits of ABC superfamily: ATP-binding components	−2.1	Putative ATP-binding component of a transport system
sugE	Multidrug efflux system protein	−2.1	Suppresses groEL, may be chaperone
ybbD	pseudo	−2.1	orf, hypothetical protein
yjhI	KpLE2 phage-like element; predicted DNA-binding transcriptional regulator	−2.1	Putative regulator
glcF	Glycolate oxidase iron-sulfur subunit	−2.1	Glycolate oxidase iron-sulfur subunit
ybdO	Predicted DNA-binding transcriptional regulator	−2.1	Putative transcriptional regulator LYSR-type
mcrA	e14 prophage; 5-methylcytosine-specific restriction endonuclease B	−2.1	Restriction of DNA at 5-methylcytosine residues; at locus of e14 element
efeB	Conserved protein	−2.1	orf, hypothetical protein
yabP	Pseudo	−2.1	orf, hypothetical protein
arnT	4-amino-4-deoxy-L-arabinose transferase	−2.1	orf, hypothetical protein
ais	Conserved protein	−2.1	Protein induced by aluminum
rsxC	Fused predicted 4Fe-4S ferredoxin-type protein/conserved protein	−2.1	Putative membrane protein
yagU	Conserved inner membrane protein	−2.1	orf, hypothetical protein
yciF	Conserved protein	−2.1	Putative structural proteins
yifK	Predicted transporter	−2.1	Putative amino acid/amine transport protein
yncD	Predicted iron outer membrane transporter	−2.1	Putative outer membrane receptor for iron transport
yhcO	Predicted barnase inhibitor	−2.1	orf, hypothetical protein
elaD	Predicted enzyme	−2.1	Putative sulfatase/phosphatase
eamA	Cysteine and O-acetyl-L-serine efflux system	−2.1	orf, hypothetical protein
glcD	Glycolate oxidase subunit, FAD-linked	−2.1	Glycolate oxidase subunit D
ydgC	Conserved inner membrane protein associated with alginate biosynthesis	−2.2	orf, hypothetical protein
sugE	Multidrug efflux system protein	−2.2	Suppresses groEL, may be chaperone
alsC	D-allose transporter subunit	−2.2	Putative transport system permease protein
yifK	Predicted transporter	−2.2	Putative amino acid/amine transport protein
yhhY	Predicted acetyltransferase	−2.2	orf, hypothetical protein
fhuB	Fused iron-hydroxamate transporter subunits of ABC superfamily: membrane components	−2.2	Hydroxamate-dependent iron uptake, cytoplasmic membrane component
hdeB	Acid-resistance protein	−2.2	orf, hypothetical protein
yfhA	Predicted DNA-binding response regulator in two-component system	−2.2	Putative 2-component transcriptional regulator
glgS	Predicted glycogen synthesis protein	−2.2	Glycogen biosynthesis, rpoS dependent
ydaQ	Rac prophage; conserved protein	−2.2	orf, hypothetical protein
ylbH	Pseudo	−2.2	orf, hypothetical protein
rfaP	Kinase that phosphorylates core heptose of lipopolysaccharide	−2.2	Lipopolysaccharide core biosynthesis; phosphorylation of core heptose
stpA	DNA binding protein, nucleoid-associated	−2.2	DNA-binding protein; H-NS-like protein; chaperone activity
lpxT	Undecaprenyl pyrophosphate phosphatase	−2.2	orf, hypothetical protein
ydhY	Predicted 4Fe-4S ferridoxin-type protein	−2.2	Putative oxidoreductase, Fe-S subunit
yifK	Predicted transporter	−2.2	Putative amino acid/amine transport protein
hisP	Histidine/lysine/arginine/ornithine transporter subunit	−2.2	ATP-binding component of histidine transport
yhgE	Predicted inner membrane protein	−2.2	Putative transport
thiQ	Thiamin transporter subunit	−2.2	Putative ATP-binding component of a transport system
ycgZ	Predicted protein	−2.2	orf, hypothetical protein
glcG	Conserved protein	−2.2	orf, hypothetical protein

(*Continued*)

Table S3 (*Continued*)

Gene name	Gene product	Fold change AgNP-ZM vs zeolite	Description
fliP	Flagellar biosynthesis protein	–2.2	Flagellar biosynthesis
yibF	Predicted glutathione S-transferase	–2.2	Putative S-transferase
rpiR	DNA-binding transcriptional repressor	–2.4	Transcriptional repressor of rpiB expression
yojI	Fused predicted multidrug transport subunits of ABC superfamily	–2.4	Putative ATP-binding component of a transport system
hsdS	Specificity determinant for hsdM and hsdR	–2.4	Specificity determinant for hsdM and hsdR
racR	Rac prophage; predicted DNA-binding transcriptional regulator	–2.4	orf, hypothetical protein
yceI	Predicted protein	–2.4	orf, hypothetical protein
tonB	Membrane spanning protein in TonB-ExbB-ExbD complex	–2.4	Energy transducer; uptake of iron, cyanocobalimin; sensitivity to phages
rfaS	Lipopolysaccharide core biosynthesis protein	–2.5	Lipopolysaccharide core biosynthesis
rutB	Predicted enzyme	–2.5	Putative synthetase
yciI	Predicted enzyme	–2.5	orf, hypothetical protein
wzyE	Predicted Wzy protein involved in ECA polysaccharide chain elongation	–2.5	TDP-Fuc4NAc:lipidII transferase; synthesis of enterobacterial common Ag
nth	DNA glycosylase and apyrimidinic (AP) lyase (endonuclease III)	–2.5	Endonuclease III; specific for apurinic and/or apyrimidinic sites
yncC	Predicted DNA-binding transcriptional regulator	–2.5	orf, hypothetical protein
yifK	Predicted transporter	–2.5	Putative amino acid/amine transport protein
yjhB	KpLE2 phage-like element; predicted transporter	–2.5	Putative transport protein
yhjR	Conserved protein	–2.5	orf, hypothetical protein
yfdI	CPS-53 (KpLE1) prophage; predicted inner membrane protein	-2.5	putative ligase
yifN	pseudo	–2.6	orf, hypothetical protein
caiF	DNA-binding transcriptional activator	–2.6	Transcriptional regulator of cai operon
flgA	assembly protein for flagellar basal-body periplasmic P ring	–2.6	Flagellar biosynthesis; assembly of basal-body periplasmic P ring
serA	D-3-phosphoglycerate dehydrogenase	–2.6	D-3-phosphoglycerate dehydrogenase
can	Carbonic anhydrase	–2.7	Putative carbonic anhdrase
yacC	Predicted protein	–2.7	orf, hypothetical protein
ydbL	Conserved protein	–2.7	orf, hypothetical protein
efeO	Conserved protein	–2.7	orf, hypothetical protein
fliF	Flagellar basal-body MS-ring and collar protein	–2.7	Flagellar biosynthesis; basal-body MS
flgC	Flagellar component of cell-proximal portion of basal-body rod	–2.7	Flagellar biosynthesis, cell-proximal portion of basal-body rod
can	Carbonic anhydrase	–2.7	Putative carbonic anhdrase
rsxD	Predicted inner membrane oxidoreductase	–2.7	orf, hypothetical protein
fliM	Flagellar motor switching and energizing component	–2.7	Flagellar biosynthesis, component of motor switch and energizing
ybaN	Conserved inner membrane protein	–2.8	Putative gene 58
proV	Glycine betaine transporter subunit	–2.8	ATP-binding component of transport system for glycine, betaine and proline
fhuD	Iron-hydroxamate transporter subunit	–2.8	Hydroxamate-dependent iron uptake, cytoplasmic membrane component
can	Carbonic anhydrase	–2.8	Putative carbonic anhdrase
sufE	Sulfur acceptor protein	–2.8	orf, hypothetical protein
sufS	Selenocysteine lyase, PLP-dependent	–2.8	orf, hypothetical protein
ariR	Predicted protein	–2.8	orf, hypothetical protein
wcaM	Predicted colanic acid biosynthesis protein	–2.8	orf, hypothetical protein
ymgA	Predicted protein	–2.9	orf, hypothetical protein

(*Continued*)

Table S3 (*Continued*)

Gene name	Gene product	Fold change AgNP-ZM vs zeolite	Description
ybiX	Conserved protein	–2.9	Putative enzyme
yacC	Predicted protein	–2.9	orf, hypothetical protein
sufC	Component of SufBCD complex, ATP-binding component of ABC superfamily	–2.9	Putative ATP-binding component of a transport system
can	Carbonic anhydrase	–2.9	Putative carbonic anhydrase
yacC	Predicted protein	–3	orf, hypothetical protein
fhuC	Iron-hydroxamate transporter subunit	–3	ATP-binding component of hydroxymate-dependent iron transport
sodA	Superoxide dismutase, Mn	–3.1	Superoxide dismutase, manganese
can	Carbonic anhydrase	–3.2	Putative carbonic anhydrase
cbrB	Predicted inner membrane protein	–3.2	orf, hypothetical protein
flgB	Flagellar component of cell-proximal portion of basal-body rod	–3.3	Flagellar biosynthesis, cell-proximal portion of basal-body rod
ompT	DLP12 prophage; outer membrane protease VII (outer membrane protein 3b)	–3.3	Outer membrane protein 3b
rsxE	Predicted inner membrane NADH-quinone reductase	–3.3	orf, hypothetical protein
pqqL	Predicted peptidase	–3.3	Putative peptidase
fliA	RNA polymerase, sigma 28 (sigma F) factor	–3.3	Flagellar biosynthesis; alternative sigma factor 28
yfdH	CPS-53 (KpLE1) prophage; bactoprenol glucosyl transferase	–3.5	Putative glycan biosynthesis enzyme
yjgL	Predicted protein	–3.5	orf, hypothetical protein
sufD	Component of SufBCD complex	–3.7	orf, hypothetical protein
yfdH	CPS-53 (KpLE1) prophage; bactoprenol glucosyl transferase	–3.7	Putative glycan biosynthesis enzyme
fepB	Iron-enterobactin transporter subunit	–3.7	Ferric enterobactin
fliL	Flagellar biosynthesis protein	–3.7	Flagellar biosynthesis
sufB	Component of SufBCD complex	–3.7	orf, hypothetical protein
sufA	Fe-S cluster assembly protein	–3.8	orf, hypothetical protein
ycgF	Predicted FAD-binding phosphodiesterase	–3.8	orf, hypothetical protein
yfdH	CPS-53 (KpLE1) prophage; bactoprenol glucosyl transferase	–3.8	Putative glycan biosynthesis enzyme
sufA	Fe-S cluster assembly protein	–3.9	orf, hypothetical protein
ybdB	Conserved protein	–4	orf, hypothetical protein
fhuE	Ferric-rhodotorulic acid outer membrane transporter	–4	Outer membrane receptor for ferric iron uptake
sufA	Fe-S cluster assembly protein	–4.3	orf, hypothetical protein
yfdH	CPS-53 (KpLE1) prophage; bactoprenol glucosyl transferase	–4.4	Putative glycan biosynthesis enzyme
exbD	Membrane spanning protein in TonB-ExbB-ExbD complex	–4.5	Uptake of enterochelin; tonB-dependent uptake of B colicins
yncE	Conserved protein	–4.5	Putative receptor
fepD	Iron-enterobactin transporter subunit	–4.7	Ferric enterobactin
sufA	Fe-S cluster assembly protein	–4.9	orf, hypothetical protein
entB	Isochorismatase	–5	2,3-dihydro-2,3-dihydroxybenzoate synthetase, isochroismatase
entC	Isochorismate synthase 1	–5.3	Isochorismate hydroxymutase 2, enterochelin biosynthesis
tdcA	DNA-binding transcriptional activator	–5.3	Transcriptional activator of tdc operon
fepA	Iron-enterobactin outer membrane transporter	–5.4	Outer membrane receptor for ferric enterobactin
fepC	Iron-enterobactin transporter subunit	–5.6	ATP-binding component of ferric enterobactin transport
fes	Enterobactin/ferric enterobactin esterase	–5.6	Enterochelin esterase
exbB	Membrane spanning protein in TonB-ExbB-ExbD complex	–5.8	Uptake of enterochelin; tonB-dependent uptake of B colicins

(*Continued*)

Table S3 (*Continued*)

Gene name	Gene product	Fold change AgNP-ZM vs zeolite	Description
nrdH	Glutaredoxin-like protein	–5.8	Glutaredoxin-like protein; hydrogen donor
fecR	KpLE2 phage-like element; transmembrane signal transducer for ferric citrate transport	–5.9	Regulator for fec operon, periplasmic
entS	Predicted transporter	–6.6	Putative transport
entF	Enterobactin synthase multienzyme complex component, ATP-dependent	–6.8	ATP-dependent serine activating enzyme
cirA	Ferric iron-catecholate outer membrane transporter	–7.1	Outer membrane receptor for iron-regulated colicin I receptor; porin
entA	2,3-dihydro-2,3-dihydroxybenzoate dehydrogenase	–7.2	2,3-dihydro-2,3-dihydroxybenzoate dehydrogenase
entE	2,3-dihydroxybenzoate-AMP ligase component of enterobactin synthase multienzyme complex	–7.4	2,3-dihydroxybenzoate-AMP ligase
yddB	Predicted porin protein	–7.9	orf, hypothetical protein
fecI	KpLE2 phage-like element; RNA polymerase, sigma 19 factor	–8.5	Probable RNA polymerase sigma factor
nrdI	Protein that stimulates ribonucleotide reduction	–8.8	orf, hypothetical protein
ydiE	Conserved protein	–9.2	orf, hypothetical protein
nrdE	Ribonucleoside-diphosphate reductase 2, alpha subunit	–10.4	Ribonucleoside-diphosphate reductase 2, alpha subunit
bfd	Bacterioferritin-associated ferredoxin	–10.6	orf, hypothetical protein
yddA	Fused predicted multidrug transporter subunits of ABC superfamily	–12.4	Putative ATP-binding component of a transport system
fepG	Iron-enterobactin transporter subunit	–12.6	Ferric enterobactin transport protein
fiu	Predicted iron outer membrane transporter	–13.7	Putative outer membrane receptor for iron transport
nrdF	Ribonucleoside-diphosphate reductase 2, beta subunit, ferritin-like protein	–13.9	Ribonucleoside-diphosphate reductase 2, beta chain, frag
fhuF	Ferric iron reductase involved in ferric hydroximate transport	–17.6	orf, hypothetical protein

Supplemental References

1. Gentleman RC, Carey VJ, Bates DM et al. Bioconductor: Open software development for computational biology and bioinformatics. *Genome Biol*. 2004;5(10):R80.
2. Tusher VG, Tibshirani R, Chu G. Significance analysis of microarrays applied to the ionizing radiation response. *Proc Natl Acad Sci U S A*. 2001;98(9):5116–5121.
3. Storey JD, Tibshirani, R. Statistical significance for genomewide studies. *Proc Natl Acad Sci U S A*. 2003;100(16):9440–9445.